Structural Engineering and Mechanics, *Vol. 72, No. 3 (2019) 355-366*
DOI: https://doi.org/10.12989/sem.2019.72.3.355

Analytical investigation on lateral load responses of self-centering walls with distributed vertical dampers

Xiaogang Huang, Zhen Zhou* and Dongping Zhu

Key Laboratory of Concrete and Prestressed Concrete Structures of the Ministry of Education, Southeast University, Nanjing, China

(Received April 10, 2019, Revised June 10, 2019, Accepted June 12, 2019)

Abstract. Self-centering wall (SCW) is a resilient and sustainable structural system which incorporates unbonded posttensioning (PT) tendons to provide self-centering (SC) capacity along with supplementary dissipators to dissipate seismic energy. Hysteretic energy dissipators are usually placed at two sides of SCWs to facilitate ease of postearthquake examination and convenient replacement. To achieve a good prediction for the skeleton curve of the wall, this paper firstly developed an analytical investigation on lateral load responses of self-centering walls with distributed vertical dampers (VD-SCWs) using the concept of elastic theory. A simplified method for the calculation of limit state points is developed and validated by experimental results and can be used in the design of the system. Based on the analytical results, parametric analysis is conducted to investigate the influence of damper and tendon parameters on the performance of VD-SCWs. The results show that the proposed approach has a better prediction accuracy with less computational effects than the Perez method. As compared with previous experimental results, the proposed method achieves up to 60.1% additional accuracy at the effective linear limit (DLL) of SCWs. The base shear at point DLL is increased by 62.5% when the damper force is increased from 0kN to 80kN. The wall stiffness after point ELL is reduced by 69.5% when the tendon stiffness is reduced by 75.0%. The roof deformation at point LLP is reduced by 74.1% when the initial tendon stress is increased from $0.45f_{pu}$ to $0.65f_{pu}$.

Keywords: self-centering walls; vertical dampers; lateral load responses; limit states; parametric analysis

1. Introduction

Traditional structural design allows occurrence of flexural plastic hinges resulting from yielding of structural members to dissipate seismic energy (Bai and Lin *et al*. 2015, Xue *et al*. 2017, 2018). Residual drift and permanent deformation are subsequently formed in the buildings after strong earthquakes. The requirements of economic considerations in terms of repair costs have triggered many researchers to develop sustainable structural systems with self-centering (SC) characteristics. Posttensioning (PT) techniques are therefore implemented into different structures by different methods to develop a number of SC systems, such as SC beam-column connections (Garlock *et al*. 2005, Kim *et al*. 2008), SC braces (Zhou *et al*. 2015, Qiu and Zhu *et al*. 2017), SC beams (Maurya and Eatherton 2016, Huang *et al*. 2017) and SC walls (Eatherton *et al*. 2014, Guo *et al*. 2014, 2017).

Self-centering walls (SCWs) are an extended evolution of rocking concepts (Priestley and Tao, 1993), which can rock about their foundation and recenter upon unloading. Armouti (1993) experimentally investigated the hysteretic performance of SCWs, demonstrating SCWs have excellent self-centering capability. Kurama *et al* (1999) analyzed the behavior of SCWs under cyclic lateral loads and developed a seismic design approach for SCWs. Kurama *et al* (2002) continue to analyze the seismic responses of SCWs and verify the design methodology to prevent shear slip along horizontal joints in walls. The results showed that the tendon area, initial force and tendon eccentricity had significant influence on the SC capability. They also indicated that the method for estimating wall drifts needed to be improved. Perez *et al*. (2004a, 2004b, 2007, 2013) derived a series of closed-form expressions on the behavior of SCWs and then proposed a design method for SCWs based on experimental and numerical investigation. Moreover, Perez *et al*. (2004c) described the lateral load behavior of SCWs with vertical joint connectors using a trilinear load-displacement response curve and divided skeleton curves of SCWs in four main limited states: (1) decompression at the base of the wall (DEC), (2) effective limit of the linear-elastic response of the wall (ELL), (3) yielding of posttensioning steel (LLP) and (4) crushing of confined concrete (CCC). Aaleti and Sritharan (2009) analyzed a jointed wall system and proposed a simplified method to estimate the behavior of this wall system, which can capture the behavior of walls, as well as the natural axis depth at wall base, elongation of unbonded posttensioning (PT) tendons and connector deformation in vertical joints. Hu *et al* (2013) studied the seismic behavior of SCWs intended for use in seismic retrofit of reinforced concrete (RC) frame structures. Abdalla *et al*. (2014) optimized the seismic design process of SCWs using artificial natural network (ANN) approach. The proposed ANN model could predict the non-dimensioned optimum design parameters

*Corresponding author, Professor
E-mail: seuhj@163.com

http://www.techno-press.com/journals/sem&subpage=7
ISSN: 1225-4568 (Print), 1598-6217 (Online)

related to the area of PT tendons and the yield force of shear connectors while avoiding a complicated iterative process.

SCWs usually displayed nonlinear elastic responses with limited energy dissipation capacity whereas SCWs incorporating supplementary dissipators exhibited stable flag-shaped hysteretic behaviors. Kurama (2000) added linear viscous fluid dampers as passive energy dissipation system into SCWs. He proposed a design approach to control the maximum roof drift of SCWs with viscous dampers and verified the performance of wall systems through nonlinear dynamic time-history analysis. Kurama (2001) added supplementary friction dampers along the vertical joint between two separate walls. Analysis results found that friction dampers can significantly reduce the maximum displacement of SCWs. Then he also proposed a simplified seismic design approach to control the peak roof drift below an allowable target displacement. Restrepo and Rahman (2007) added mild steel bars between wall and foundation. Experimental results showed that its hysteretic curve is typical flag-shape, and mild steel bars can improve the energy dissipation capacity of walls without influencing the SC ability. Furthermore, Bayat *et al* (2011a, 2011b, 2014) has suggested supplementary dissipators such as yielding dampers are capable of reducing earthquake-induced structural responses under both far field and near field records.

Despite the benefits of the new wall system, only limited research has established theoretical methods to predict the lateral load behavior of SCWs (Perez *et al*. 2004c). Furthermore, there are some limitations identified with the previous method: (1) neglecting the effects of gap opening between point DEC and point ELL on the lateral load responses and therefore cannot achieve a good prediction on point ELL; (2) adopting a complex iteration process to calculate point LLP. The motivation of this paper is to build upon the previous methods and bring forward that the lateral load responses of SCWs with distributed vertical dampers (VD-SCWs) can be calculated using the concept of elastic theory. Closed-form solutions to analyze the lateral load behavior of VD-SCWs are presented. The prediction accuracy for point ELL is improved by including the gap opening effect at the base upon uplifting of the walls. A simplified solution is proposed for point LLP to avoid iterative calculation in the previous methods. After verifying the proposed equations of VD-SCWs by experimental results, parametric analysis is conducted to investigate the influence of PT tendons and damper parameters on the lateral load responses of VD-SCWs.

2. Elastic solution of VD-SCWs

Cast-in-place concrete walls have been widely used as the lateral-load resisting system in seismic regions, which achieve a highly ductile capacity through large inelastic deformations. This means the walls will retain permanent damage and residual deformation after experiencing strong earthquakes, resulting in higher economic loss and post-earthquake repairs. VD-SCWs that incorporate unbonded posttensioning tendons to provide a recentering capacity along with distributed vertical dampers to dissipate seismic energy are proposed to solve these issues. The purpose of VD-SCWs is to provide high performance options for projects where owners want reduced structural damages, repair costs, and business downtime. One of the big benefits of VD-SCWs is that the total strength can be “tuned” to the demands of the traditional walls by adjusting initial posttensioning force and damper activation force. Therefore, VD-SCWs can be designed to achieve a goal of reaching similar peak story drift while eliminating residual drift compared to traditional walls. Although current literatures lacks of a detailed comparison of costs between VD-SCWs and traditional walls, the costs of VD-SCWs will not significantly higher than regular construction considering its advantage of reduced on-site construction.

Fig.1(a) shows the schematic of wall-frame structure, constructed by linking a rocking wall with moment frames at two sides of the wall. Unbonded PT tendons, which provide a restoring force to the system, pass vertically through the panels with one end anchored at the foundation and the other at the top of the wall. Distributed VD are installed along the vertical joints between the wall and adjacent frame columns. The two main functions of VD are: (1) connect the wall and column together and (2) dissipate seismic energy primarily. The recentering responses of the system are achieved when the pertinent moment resulting from the pretension of tendons overcomes the moment from dampers. Fig. 1(b) illustrates the kinematics of the system when it is loaded to the right direction. SCWs are assumed to remain essentially elastic at the beginning of uplifting at the column bases. Once uplifting has occurred, the wall rocks about the pivoting point at one edge of the base and gap occurred along the horizontal joint at the other edge of the wall, causing an elongation of the tendons. The energy dissipation mechanism of VD act based on relative vertical displacements of the wall and column interface upon uplifting. Different types of dissipators can be used for energy dissipation such as yielding dampers (Fig. 1(c)) or friction dampers (Fig. 1(d)). The friction dampers are comprised of two steel angles and one T-shaped section, which are bolted to the column and the wall respectively (Guo *et al*. 2014). After the applied load disappears, the PT tendons provide additional force to recenter the system to its initial position. Therefore, VD-SCWs have stable energy dissipation levels while maintaining SC capability under lateral loading.

The SC capacity of the wall is achieved by providing sufficient pretension in the tendons, in addition to the wall gravity, to compress the dampers to near zero strain when the loading is removed. The SC ratio is thus defined as the ratio of restoring moment provided by the initial PT force in the tendons and gravity loads, to the resisting moment provided by the yielding dampers. A SC ratio larger than 1 is usually designed to ensure the SC capacity of the wall. However, with continued loading, the occurrence of yielding in the tendons will lead to a loss of pretension and subsequently cause the system to lose its SC capability, which should be delayed as much as possible during the rocking process of the wall. Therefore, PT tendons are usually required to keep elastic in the design process of VD-SCWs under design basis earthquakes, but may experience plastic deformation after exceeding maximum considered earthquakes.

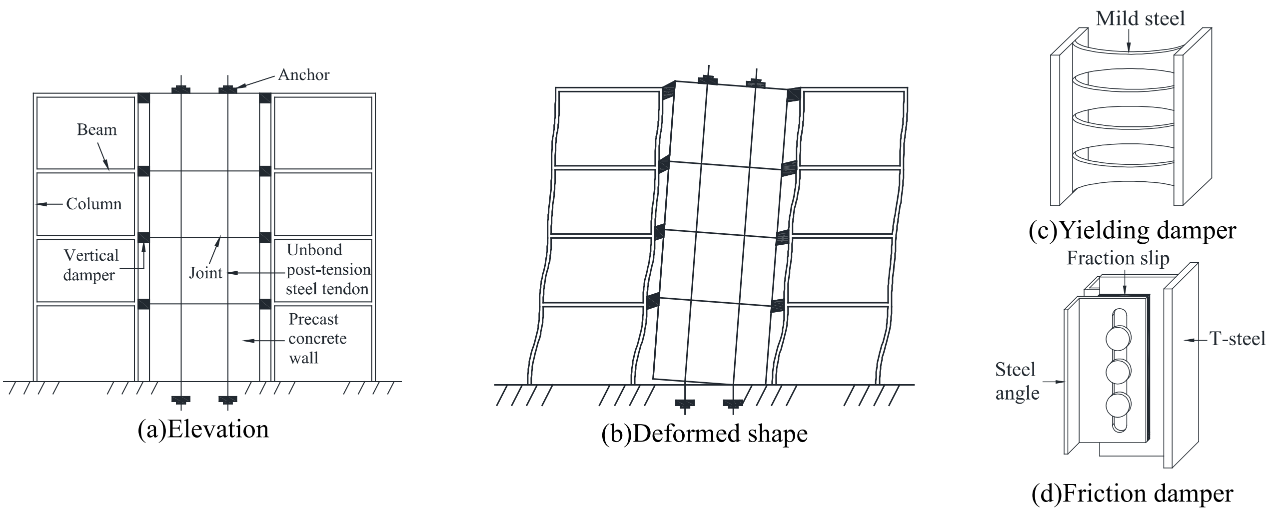

Fig. 1 The concept of wall-frame structure with vertical dampers

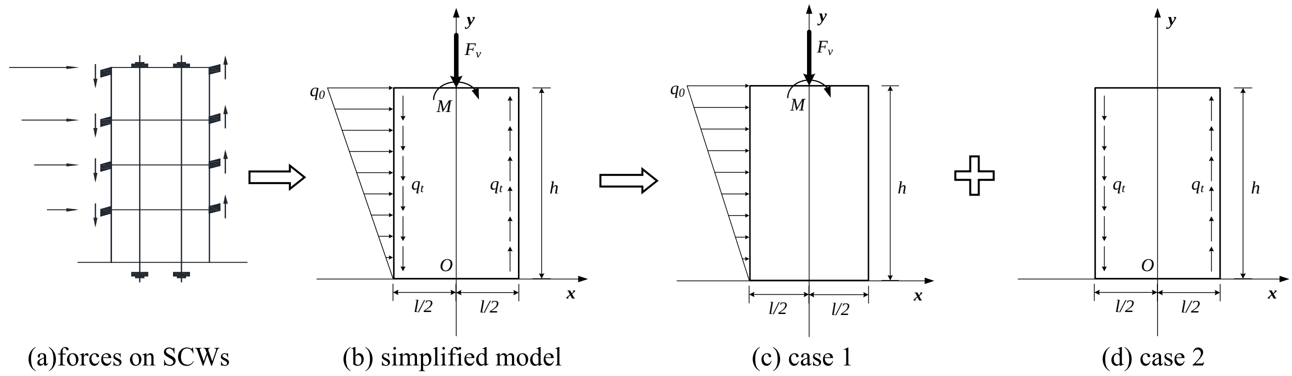

Fig. 2 Analytical model of VD-SCWs

2.1 Analytical model

Fig.2(a) shows the configuration and load patterns of VD-SCWs. According to some experimental and analytical results of SCWs (Perez 2004a), the following assumptions are used to analyze the lateral load responses of VD-SCWs: (1) The wall has sufficient out-of-plane bracing system to prevent its out-plane buckling. (2) The foundation is strong enough to support the wall during the whole loading process. (3) The wall body keeps elastic in the whole analysis process. (4) Horizontal slipping of the wall is ignored. The shear friction capacity at the wall-to-foundation connections is assumed greater than the maximum wall base shear demands. A criterion developed by Kurama *et al*. (2002) can be used to estimate this demand. (5) The failure of vertical dampers and tendon anchors are not considered. (6) The prestress loss in tendons are neglected. (7) PT tendons are placed symmetrically in the wall. Fig. 2(b) shows a plot of the simplified analytical model.

As shown in Fig. 2(b), h is the height of wall, and l is the width of wall. q_0 represents the lateral load on the wall and is assumed as inverted triangle pattern, considering the distribution of seismic loading. Other kinds of load patterns can be transformed to q_0 by equivalent total base shear and equivalent total moment. For example, the concentrated load V at the top of wall can be transformed equivalently through Eq.(1)

$$q_0 = \frac{2V}{h}\ ,\ M_{eq} = \frac{Vh}{3} \tag{1}$$

Two vertical sides of wall are considered as the main boundary. The equivalent vertical load at both vertical sides (q_t) generated by the dampers are calculated as Eq.(2)

$$q_t = \begin{cases} \dfrac{ndk_d}{h} & d \le d_y \\ \dfrac{nF_{dy}}{h} & d > d_y \end{cases} \tag{2}$$

The top side of wall is considered as the secondary boundary and loads applied on it can be simplified as F_v and M. F_v denotes the total forces in PT tendons. M is the total moment generated by uneven tendon forces (M_p) and lateral loading equivalization (M_{eq}), as following

$$M = M_p + M_{eq} \tag{3}$$

where n is the number of dampers on each side of wall; d is the vertical displacement of dampers; d_y is the yield displacement of dampers; k_d is the elastic stiffness of dampers; F_{dy} is the yield force of dampers.

2.2 Elastic solution

For facilitating the derivation of equations, loading effects and boundary conditions in the theoretical model (Fig. 2(b)) are divided into two cases. Case 1 shown in Fig. 2(c) considers the effect of lateral load (q_0) and secondary boundary load at top of the wall (F_v, M). Case 2 shown in Fig.2(d) considers the effect of damper forces and the self-weight of wall. The total responses of VD-SCWs can be obtained by the summation of the two cases.

2.2.1 Case 1

The normal stress of the wall along x-direction in case 1 (σ_{x1}) is derived by the following equation

$$\sigma_{x1} = \frac{\partial^2 \Phi}{\partial y^2} = y f(x) \tag{4}$$

where Φ is the stress function which is calculated by Eq.(5)

$$\Phi = \frac{1}{6} y^3 f(x) + y f_1(x) + f_2(x) \tag{5}$$

where $f(x)$, $f_1(x)$ and $f_2(x)$ are determined by compatible equations ($\nabla^4\Phi=0$) and boundary conditions (q_0, F_v, and M). Then the stress function can be solved and the corresponding solutions are given as follows

$$\sigma_{y1} = \frac{-5F_v hl^2 + q_0 a_1 x - 60Mhx}{5hl^3} \tag{6}$$

$$\sigma_{x1} = -\frac{q_0 (l-2x)^2 (l+x) y}{2hl^3} \tag{7}$$

$$\tau_{xy1} = \frac{-q_0 (l^2 - 4x^2)(-60h^2 + l^2 - 20x^2 + 60y^2)}{80hl^3} \tag{8}$$

where σ_{y1} is the normal stress along y-direction in case 1; τ_{xy1} is the shear stress in y-direction of x-surface under load pattern 1; a_1 is expressed as following

$$a_1 = -20h^3 + 30yh^2 - 3yl^2 + 20x^2 y - 10y^3 \tag{9}$$

2.2.2 Case 2

Case 2 considers the effects of gravity and the boundary conditions of damper forces. The stress solution is derived in the same way in the Case 1,

$$\sigma_{x2} = 0 \tag{10}$$

$$\sigma_{y2} = \frac{12 q_t x (h-y)}{l^2} - \rho g (h-y) \tag{11}$$

$$\tau_{xy2} = q_t \left(-\frac{1}{2} + \frac{6x^2}{l^2} \right) \tag{12}$$

where σ_{x2} and σ_{y2} are the normal stress along x-direction and y-direction in case 2, respectively; τ_{xy2} is the shear stress along y-direction of x-surface; ρ is the density of the concrete wall; g is the gravitational acceleration.

2.2.3 Elastic solution of the wall

With superposition of the results of above two cases, the elastic stress solutions of VD-SCWs can be obtained as

$$\sigma_x = \sigma_{x1} \ , \ \sigma_y = \sigma_{y1} + \sigma_{y2} \ , \ \tau_{xy} = \tau_{xy1} + \tau_{xy2} \tag{13}$$

Then the deformation of VD-SCWs can be solved. To simplify the calculation, the effect of poisson ratio is not considered since most part of wall body keeps in elastic state. The geometric equation are

$$\varepsilon_x = \frac{\partial u}{\partial x} \ , \ \varepsilon_y = \frac{\partial v}{\partial y} \ , \ \gamma_{xy} = \frac{\partial u}{\partial y} + \frac{\partial v}{\partial x} \tag{14}$$

where ε_x and ε_y are normal strain in x- and y- direction respectively; u and v are x- and y- direction displacement of wall respectively; γ_{xy} is the shear strain of wall.

By integrating the normal strain and considering the compatible of shear strain, the displacement solution can be solved as follows

$$u(x,y) = \frac{1}{20E_c hl^3}\left(b_1 q_0 + c_1 q_t + 120hy^2 M\right) \tag{15}$$

$$v(x,y) = -\frac{1}{40E_c hl^3}\left(d_1 q_0 + e_1 q_t + 40hl^2 y F_v + 480hxyM + f_1\right) \tag{16}$$

where E_c is elasticity modulus of the concrete, the other parameters in the above equations are expressed as follows;

$$\begin{aligned}
b_1 &= y\begin{pmatrix} -10l^3 x + l^2\left(15x^2 - 8y^2\right) \\ +2\left(-5x^4 + 20h^3 y - 10h^2 y^2 + y^4\right) \end{pmatrix} \\
c_1 &= -40hl(3h - y)y^2 \\
d_1 &= \begin{pmatrix} -60h^2 l^2 x + 80h^2 x^3 + 160h^3 xy - 120h^2 xy^2 \\ +x\begin{pmatrix} l^4 - 10l^3 x + 2l^2\left(x^2 + 6y^2\right) \\ +4\left(3x^4 - 20x^2 y^2 + 5y^4\right) \end{pmatrix} \end{pmatrix} \\
e_1 &= \begin{pmatrix} 40hl^3 x - 480h^2 lxy \\ +20hl\left(-8x^3 + 12xy^2\right) \end{pmatrix} \\
f_1 &= \rho(40gh^2 l^3 y - 20ghl^3 y^2)
\end{aligned} \tag{17}$$

The horizontal displacement at the top mid-point of wall under lateral loads, L_e is obtained as

$$L_e = u(x,y)|_{x=0,y=h} = \frac{h^2\left(60M + q_0(11h^2 - 4l^2) - 40hlq_t\right)}{10E_c l^3} \tag{18}$$

Eq. (18) can be used to solve the displacement caused by the elastic deformation of wall in Section 3, but the related loads (q_0, M, q_t) should use different values of different limit states.

Table 1 Descriptions of four limit states

	Limit states	Description
①	L_{DEC} V_{DEC}	Decompression of the wall(DEC): decompression occurs at one edge of the wall base by the overturning moment due to lateral loads;
②	L_{ELL} V_{ELL}	Effective Linear Limit(ELL): apparent softening resulting from the progression of gap opening along the horizontal joint is observed in the load-displacement relationship;
③	L_{LLP} V_{LLP}	Yielding of the tendons (LLP): the steel strain of the tendons exceeds its yield strain and some prestress begins to be lost after lateral load is removed;
④	L_{CCC} V_{CCC}	Crushing of confined concrete (CCC): crushing of the confined concrete occurs when the ultimate concrete compressive strain is reached;

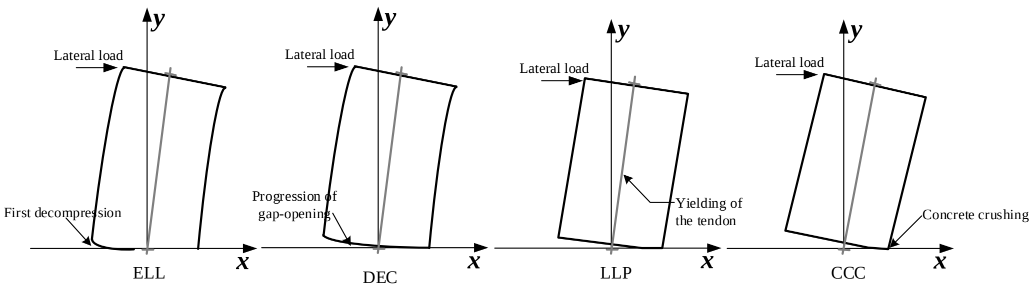

Fig. 3 Conceptual drawings showing different limit states

3. Limit state analysis

Based on the previous elastic analysis, this section introduces the derivation of expressions for calculating the base shear and roof displacement corresponding to points DEC, ELL, LLP, and CCC. Four limit states of the wall are identified in Table 1, and demonstrated graphically in Fig.3. The lateral deformations of the wall are exaggerated for purposes of demonstration. Fig.4 shows an illustration of how the expected structural capacities are related to the seismic demand levels after wall limit states are determined. The structural capacities under different designed displacement can be categorized into four groups based on wall limit states. Close-form solutions in this sections are used to facilitate the designers to calculate wall limit states within the framework of current design procedure. Once all the wall limit states are determined under the required displacement, the structural capacities can be calibrated to meet structural demands. Some information about current design of SCWs is given here for completeness, but more details can be found in Kurama *et al*. (1997, 2000, 2001). The design approach of SCWs uses two performance levels: immediate occupancy and collapse prevention. The immediate occupancy level is reached at point LLP and the collapse prevention level is reached at point CCC. The design objectives are to not exceed the immediate occupancy performance level under the design basis earthquakes and the collapse prevention performance level under the maximum considered earthquakes.

3.1 DEC State

The bottom of VD-SCWs keeps initially in full compression because the PT forces in the tendons and the wall self-weight act on the base of the wall. When the lateral load is applied, the overturning moment causes the decrease of compressive stress at one side of wall base. DEC state is defined as the occasion when the compressive stress of the edge point decreases to zero. According to $\sigma_y|_{x=-\frac{l}{2},y=0}=0$ shown in Fig. 2(b), the equation of force equilibrium at this state can be given as

$$\frac{-4q_{0,DEC}h^2-12M_{eq}+12q_t hl}{l^3}\times\left(-\frac{l}{2}\right)=\rho gh+\frac{F_v}{l} \quad (19)$$

where $q_{0,DEC}$ is the lateral load at point DEC.

By solving Eq. (19), $q_{0,DEC}$ can be obtained. Then the lateral displacement at point DEC can be calculated as

$$L_{DEC}=L_{e,DEC} \quad (20)$$

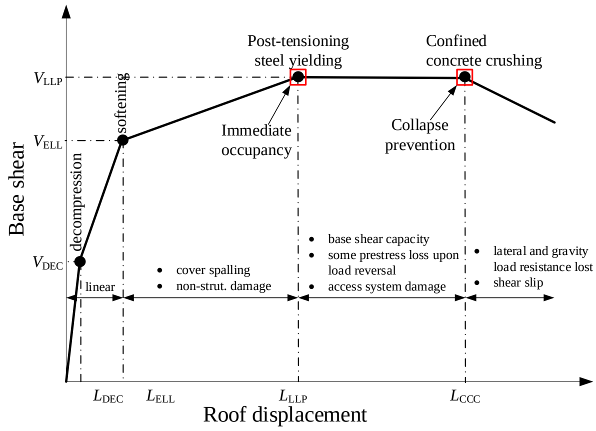

Fig. 4 Definition of wall limit states

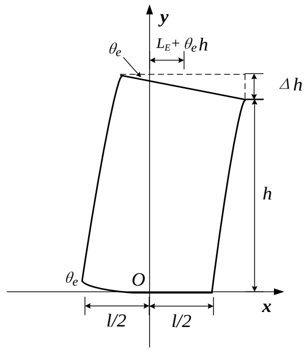

Fig.5 Influence of the gap at the joint

where $L_{e,DEC}$ is calculated by substituting $q_{0,DEC}$ into Eq. (18)

3.2 ELL State

Softening in the stiffness of SCWs will occur when the gap along the wall base at least propagates to centroidal axis of the wall (Priestley 1993). Lateral loads equal to $2q_{0,DEC}$ is required for the gap at the base of the wall to reach the wall centerline. The compression stress resultant at the base of the wall can reach the extreme compression edge of the wall when lateral load increase to $3q_{0,DEC}$. Based on fiber-based analytical models, Kurama (1997) found that the stiffness of SCWs would decrease obviously when the lateral load increase to 2.5 times of point DEC load. In this study, the lateral load $q_{0,\mathrm{ELL}}$ at point ELL is also taken equal to

$$q_{0,ELL} = 2.5q_{0,DEC} \tag{21}$$

A gap will initially open at one edge of the bottom surface in the wall after point DEC and the bottom of the wall gradually detaches from the ground base, as shown in Fig. 5. So the deformation at this state should be superposition of elastic deformation and the rotation caused by gap opening effect. However, the effect of gap opening on the lateral displacement of the wall is usually neglected in the previous studies, causing a constant initial stiffness of the wall until point ELL is reached.

A correction term for the roof displacement is proposed to include the gap opening effect along the base at point ELL, as shown in Fig. 5. It assumes that the top surface and the bottom surface of the wall are in parallel. Therefore, the rotation at the base due to the gap opening equal to the elastic rotation θ_e at the top surface.

The vertical difference between the two sides of the wall is given as follows using Eq. (16),

$$\begin{aligned}\Delta h &= v(x,y)|_{x=-\frac{l}{2},y=h} - v(x,y)|_{x=\frac{l}{2},y=h} \\ &= \frac{12h}{E_c l^2}M + \frac{3\left(80h^4 - 64h^2l^2 + 3l^4\right)}{160E_c hl^2}q_0 - \frac{6h^2}{E_c l}q_t\end{aligned} \tag{22}$$

$$\theta_e = \frac{\Delta h}{l} \tag{23}$$

where Δh = the vertical difference between the two sides of the wall, as shown in Fig. 5.

Then the correction displacement Δl at top of the wall due to θ_e is approximately given by,

$$\Delta l = \theta_e h = \frac{12h^2}{E_c l^3}M + \frac{3\left(80h^4 - 64h^2l^2 + 3l^4\right)}{160E_c l^3}q_0 - \frac{6h^3}{E_c l^2}q_t \tag{24}$$

Eq. (21) and Eq. (3) determine the values of q_0 and M. Meanwhile, the shear force q_t of the dampers can be calculated using the second formula in Eq. (2) according to the yield of the dampers in design approach due to the increase of the lateral displacement. The roof displacement of the wall L_{ELL} is the superposition of the elastic displacement and the correction displacement which is given by

$$L_{ELL} = \Delta l_{ELL} + L_{e,ELL} \tag{25}$$

where Δl_{ELL} = correction displacement using Eq. (24) at point ELL; $L_{e,ELL}$ = elastic displacement using Eq. (18) at point ELL;

3.3 LLP state

Fig. 6 shows the deformed shape of the wall at point LLP. The internal force in PT tendons will increase with the increasing overturning moment. Since PT tendons are unbonded from the wall, strain compatibility between the PT tendons and the surrounding wall does not exist. The strain in PT tendons cannot be determined by the surrounding wall deformation. Preze (2004) used an iterative method to define the contact length at the wall bottom, and calculated the natural axis which defined the relationship between force and displacement at point LLP. Aaleti and Sritharan (2009) proposed a simplified analysis method estimating natural axis depth at 2% base rotation for each wall in jointed wall system. Therefore, both the two approaches have a certain deviation in estimating the contact length of the wall. Meanwhile, the existing experiment show that the contact length at base is 18%~23% of the entire length of the wall at point LLP when the wall under appropriate initial force in PT tendons (Perez *et al*. 2007, Thomas and Sritharan 2004, Sritharan 2007). This paper simplifies the calculation base on the assumption that contact length l is almost 20% of the entire wall length shown in experiment data. The roof displacement of the wall is donated as L_{LLP} at point LLP.

The PT tendons do not yield simultaneously in all the panels due to their different arrangement location. The group of tendons locating furthest from the compression edge will yield first and point LLP is defined as the first occurrence of yielding of tendons. Thus the variation of PT force in the yielding group is expressed as the yield force subtracting the initial pretension. The PT force in the other group is also determined from similar triangles location in the wall. Rigid-body rotation θ_r at point LLP is the major factor affecting the roof displacement of the wall and the relation between the wall rotation and the total variation in PT force can be given as follows,

Table 2 Predicted results of the SCWs

Specimens	V_{DEC} (N)	L_{DEC} (mm)	V_{ELL}(N)	L_{ELL} (mm)	V_{LLP}(N)	L_{LLP} (mm)	V_{CCC}(N)	L_{CCC} (mm)
TW1/2	222737.2	5.10	556843.0	33.61	704507.3	116.80	704507.3	264.05
TW3	222737.2	3.39	556843.0	22.36	704507.3	102.57	704507.3	267.79

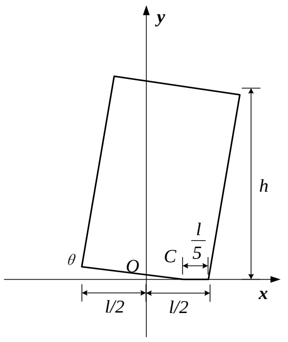

(a)Schematic of the wall

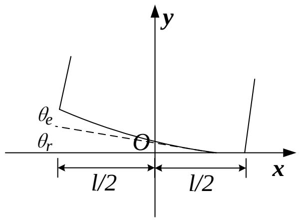

(b)Close up of the wall bottom

Fig.6 The correction of displacement at point LLP

$$\Delta F_v = A_p E_p \theta_r \left(l/2 - l/5\right)/h = \sum F_{i,LLP} - \sum F_i \quad (26)$$

where $F_{i,LLP}$ = internal force of the PT tendons at point LLP (the left steel is yield and the other internal force of steel can be linear interpolated base on the location from the point C, as shown in Fig. 6(a)); θ_r = rigid rotation of the wall which is calculated by

$$\theta_r = \frac{10h\Delta F_v}{3A_p E_p l} \quad (27)$$

The roof displacement of the wall is comprised of elastic displacement, correction displacement and rigid displacement. The lateral load $q_{0,LLP}$ is given by Eq. (28) using the moment equivalence.

$$q_{0,LLP} = \frac{3(M + q_t l)}{h^2} \quad (28)$$

where M is calculated from Eq.(3); M_p is given by

$$M_P = \sum F_{i,LLP} l_i \quad (29)$$

where l_i = the lever-arm between the tendon resultant in i group and the pivoting point.

$$L_{LLP} = \theta_{r,LLP} h + \Delta l_{LLP} + L_{e,LLP} \quad (30)$$

where $\theta_{r,LLP}$ = rigid rotation at the base of the wall calculated by Eq. (27); Δl_{LLP} = correction displacement using Eq. (24); $L_{e,LLP}$ = elastic displacement using Eq. (18).

3.4 CCC state

Crushing of the confined concrete at the compression edge occurs at point CCC, which is considered as the ultimate state of SCWs because the wall cannot sustain more lateral load with the decreasing stiffness at that time. Beyond point LLP, the small increase in the force of PT tendons compensates the decrease in the lever-arms between the pivoting points and tendon resultants. Thus lateral resistance at point CCC can be considered as constant compared to point LLP. However, the calculation of roof displacement L_{CCC} at point CCC is very complicated due to large geometric nonlinearity and plastic deformation of the wall. Following the previous methods proposed by Perez and EI-Sheikh, the rigid-body rotation at point CCC is given as follows considering the critical confined concrete crushing height h_{cr}.

$$\theta_r = \phi_{CCC} h_{cr} \quad (31)$$

$$\phi_{CCC} = \frac{\varphi \varepsilon_{cu}}{s_{CCC}} \quad (32)$$

where s_{CCC} = the length of the contact region, which is adopted as 20% of the whole length of the wall; h_{cr} = critical confined concrete crushing height, which is determined in Perez; φ = reduction factor, about 0.75-1.0.

the

$$L_{CCC} = \theta_{r,CCC} h + \Delta l_{CCC} + L_{e,CCC} \quad (33)$$

where $\theta_{r,CCC}$ = rigid-body rotation at the base of the wall calculated by Eq. (32) at point CCC; Δl_{CCC} = correction displacement using Eq. (24) at point CCC; $L_{e,CCC}$ = elastic displacement using Eq. (18) at point CCC. The yielding of PT tendons can be avoided before point CCC when θ_r satisfies the following equation,

$$\theta_r > \theta_{ccc} \quad (34)$$

Then

$$\Delta F_v > \frac{3A_p E_p l H_{cr} \varphi \varepsilon_{cu}}{10 h s_{ccc}} \quad (35)$$

4. Experiment validation

The accuracy of the proposed methods in the SCWs are validated by the experimental results of three test specimens (Perez *et al*. 2004a) including TW1, TW2 and TW3. The lateral displacement generated by the actuator was applied on the top side of the wall. TW1 was tested under monotonic load with constant gravity load, TW2 and TW3 were tested under cyclic load with constant gravity load. The load history for TW2 and TW3 was three cycles each at 0.05%, 0.1%, 0.25%, 0.5%, 0.1%, 1%, 1.5%, 2%, 0.1%, one cycle at 3%, and three additional half-cycles to the east at 3%. CCC state was not reached for TW2 due to buckling failure mode in the confined concrete region. More details about the three tested walls can be found in the precious study. (Perez *et al*. 2004a). Table 2 shows the calculated results of the walls and the test skeleton curves are given by the Fig. 7(a) to (c), where point SPL represents the spalling of the concrete in the experiments. The lateral load from the actuator is converted to inverted triangle shape using Eq. (1) in the following analysis.

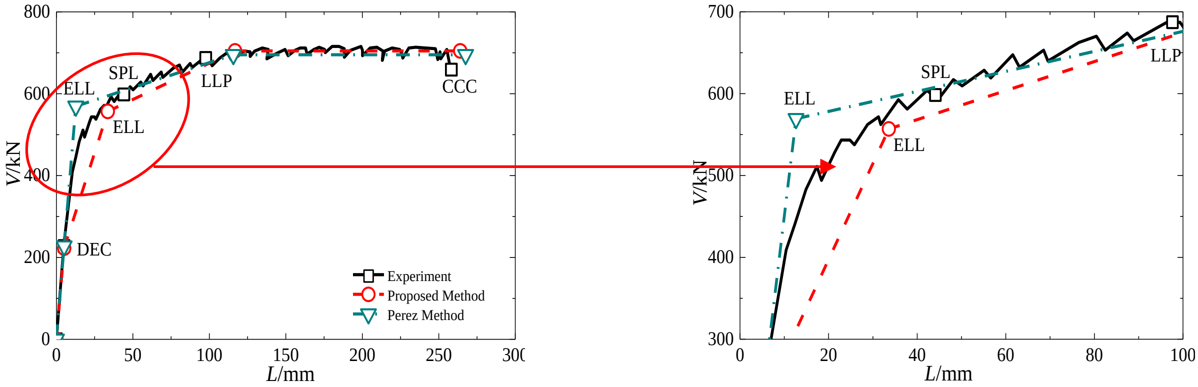

Comparison of lateral load response of TW1 based on predicted results and experiment.

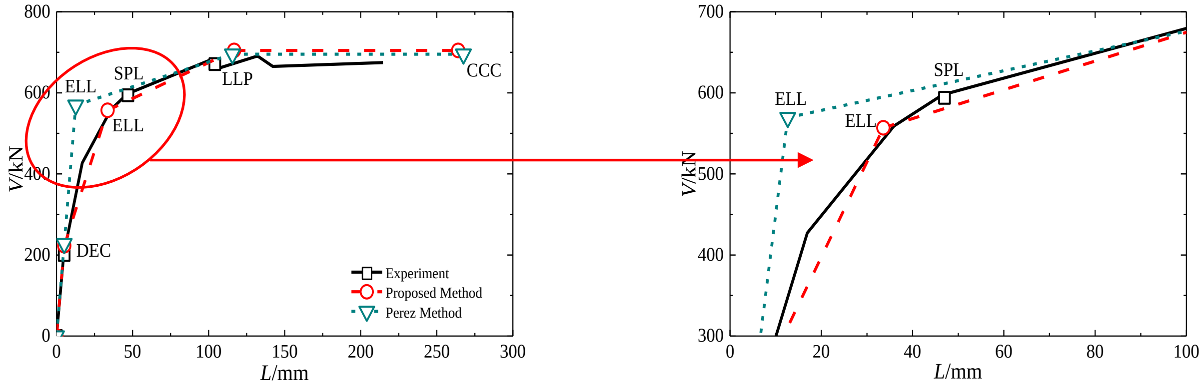

Comparison of lateral load response of TW2 based on predicted results and experiment

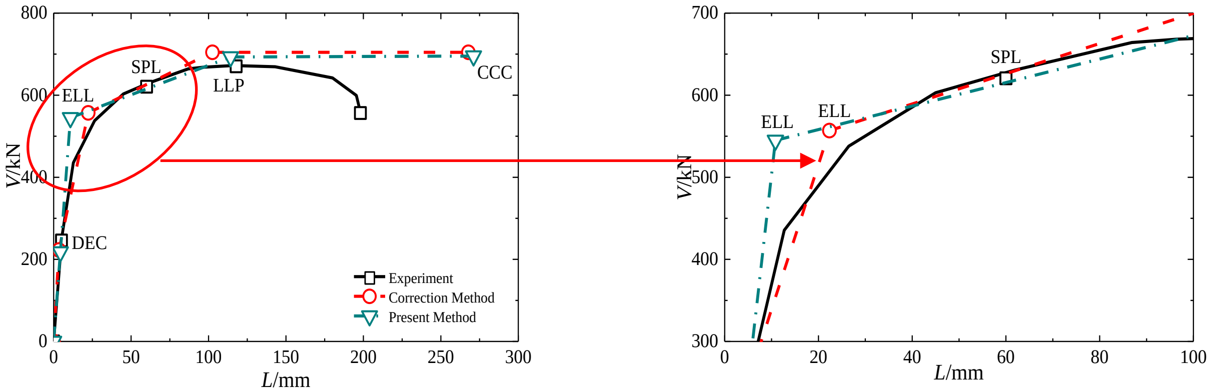

Comparison of lateral load response of TW3 based on predicted results and experiment.

Fig.7 Comparison of lateral load response of the SCWs

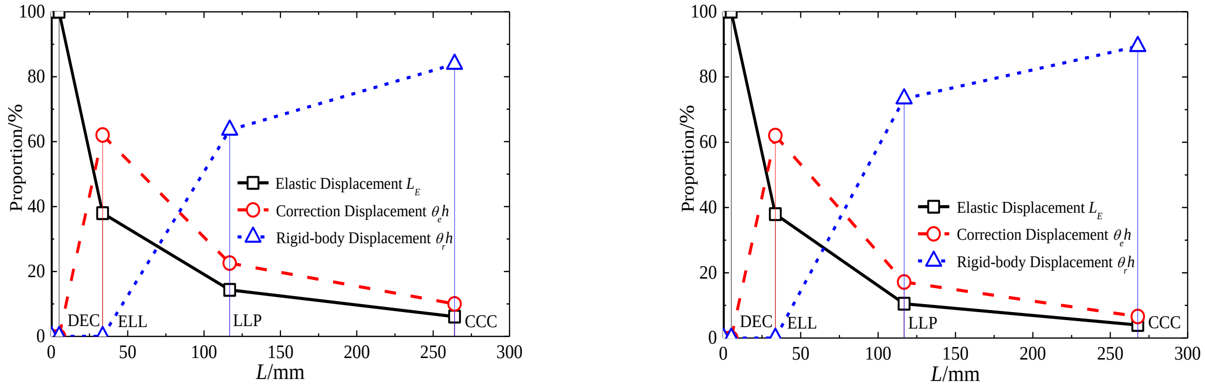

(a) The displacement proportion of TW1/TW2

(b) The displacement proportion of TW3

Fig. 8 The displacement proportion during entire loading process

As shown in Fig. 7, the proposed methods achieve a more accurate prediction of the skeleton curves in all the three test specimen compared to the Perez method (Perez *et al*, 2004a), particularly in the point ELL. The proposed method achieves up to 60.1% additional accuracy at point ELL of TW2. The lateral stiffness of the wall predicted by the Perez method beyond point DEC is obviously larger than that in the experiments. The main reason is that the effect of gap opening on the lateral displacement of the wall is neglected until point ELL is reached. Take the specimen TW2 as an example, the x-axis value of point ELL in the proposed method is 4.5% smalller than the experimental result whereas the value calculated by the Perez method is 63.9%. Moreover, the simplified method proposed in this paper has a similar accuracy with the Perez method for predicting point LLP and avoids iterative calculation process. However, the point CCC in the specimen TW2 and TW3, predicted by the two methods, obviously larger than that of the experimental results. It is an understandable deviation because the specimen TW2 and TW3 experienced cyclic loading protocol. The cyclic accumulation of strength deterioration in the wall under large cyclic displacement is difficult to be considered in the theoretical equation at point CCC.

Fig. 8 compares the percentages of elastic displacement(L_E), correction displacement($\theta_e h$) and rigid displacement($\theta_r h$) at different limit states. A close inspection of three displacement portions provides further evidence about how the different portions affect lateral displacement of the wall during the loading process. The wall is in elastic behavior before point DEC and the percentage of elastic displacement L_E is 100%. However, the percentage of correction displacement $\theta_e h$ increases to 62% and the percentage of L_E decreases to 38% at point ELL. The ratio of $\theta_e h$ to L_E is about 1.6 at point ELL, indicating the correction displacement has a large contribution on the roof displacement and should not be ignored. The percentage of rigid-body displacement $\theta_r h$ increases to more than 60% and 70% at point LLP in Fig. 8 (a) and (b) respectively. Furthermore, the percentage of $\theta_r h$ will increase to more than 80% at point CCC and become the dominant factor affecting the lateral displacement of the wall.

5. Parametric analysis

A plot of skeleton curve can give insight into the design objectives of SCWs such as initial stiffness, overstrength factors and ductility factors. Different skeleton curve of the walls can be gotten to meet different seismic performance goals by adjusting the tendon and damper properties. Based on previous theoretical anlaysis of VD-SCWs, four possible dominant parameters including activation force of damper F_{dy}, damper stiffness k_d, the initial stress of tendons f_i, the material of tendons are selected for the parametric analysis to invesitigate their effects on the skeleton curve of the wall. The specimen TW1 is studied as a benchmark model of the parametric analysis. The properties of the benchmark wall is listed in Table 3. In each parametric analysis, only one parameter is changed and the rest parameters are kept constant.

Table 3 Properties of the benchmark wall

Type	Value
Wall Parameters	parameters of TW1
Activation force of damper F_{dy}	40kN
Number of dampers	5
Initial stiffness of damper k_d	30kN/mm
Initial stress of PT tendons f_i	$0.55f_{pu}$
Material type of PT tendons	steel strand

5.1 Influence by the parameters of dampers

5.1.1 Activation force of damper

The activation force of damper dominates the energy dissipation capacity of VD-SCWs. Fig. 9 shows the skeleton curves of the VD-SCWs with five different values of the activation force of damper between 0 kN and 80 kN. All the curves overlap before point DEC regardless of damper force variations. With continued displacement, the base shear at point ELL increases significantly with the increase of damper force. The base shear at point DLL is increased by 62.5% when the damper force is increased from 0kN to 80kN. This is because the dampers installed on the sides of the wall are activated to provide energy dissipation capacity for the structure (Perez 2004c, 2004d) after the occurrence of DEC state. The other observation is the displacement in all the limit state points keeps small change, whereas obvious increase in the base shear is observed with the increase of damper activation force. This indicates that the increasing energy dissipation of dampers can reduce the possibility of exceeding point LLP where the loss of prestress occurs. Therefore, the energy-dissipation capacity of VD-SCWs needed to be increased as much as possible when the SC capacity is ensured.

5.1.2 Initial stiffness of damper

Different types of vertical dampers have different initial stiffness. It depends on the design of geometric properties of dampers. The influence of elastic stiffness on skeleton curve of the wall is investigated for the elastic stiffness values(k_d) of 20kN/mm, 30kN/mm, 40kN/mm and 300 kN/mm. The energy disspation mechanism of dampers is mainly based on the vertical relative displacement between the wall and the column interface. With an increase in k_d, damper force will increase more quickly untill the activation of dampers. However, recall from Eq. (18), the damper force q_t causes a small fraction of the lateral displacement L_e before point DEC. This can be seen in Fig. 10 that an increase in the dampers stiffness slightly affect the skeleton curve of the wall.

5.2 Influence by the parameters of PT tendons

5.2.1 Initial stress

The yielding of PT tendons is not allowed prematurely for avoiding the loss of prestress. Fig. 11 shows the skeleton curve of VD-SCWs with five different values of initial tendon stress. The increasing initial stress in PT tendons leads to an increase in the SC ratio and the lateral resistance in the point ELL. However, on the premise of maintaining a

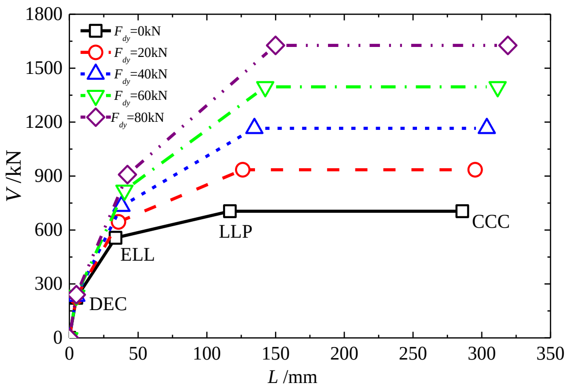

Fig. 9 Skeleton curves of VD-SCWs for different damper force

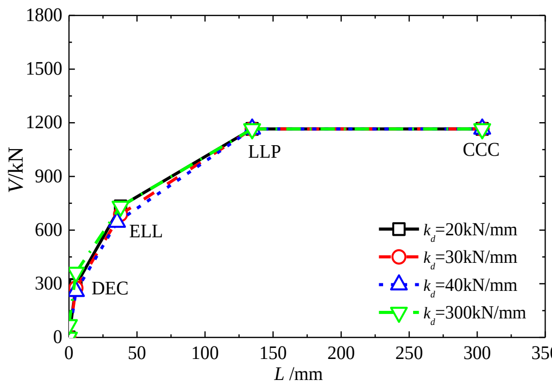

Fig. 10 Skeleton curves of VD-SCWs for different damper stiffness

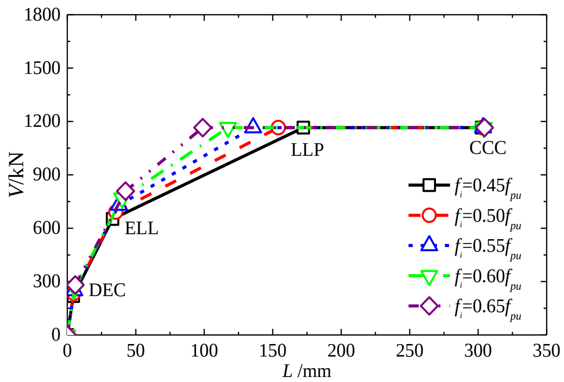

Fig. 11 Skeleton curves of VD-SCWs for different initial stress of PT tendons

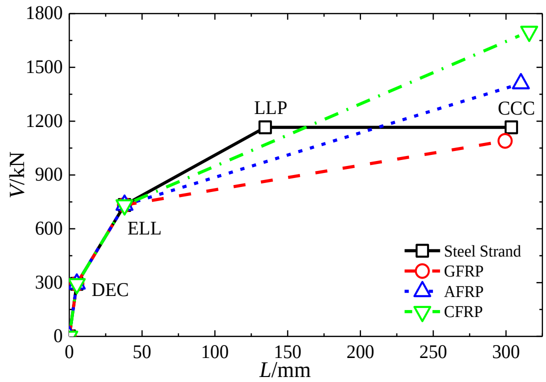

Fig. 12 Skeleton curves of VD-SCWs for different tendon material

Table 4 Material properties of the PT tendons

Type	Steel strand	GFRP	AFPR	CFRP
Ultimate tension strength/Mpa	1400~1890	480~1600	1200~2550	600~3700
Elasticity modulus/Gpa	180~200	36~65	40~125	120~580

constant tendon area, the available elastic strain of PT tendons between point ELL and LLP will decrease and the increment of PT force decreases subsequently. The roof deformation at point LLP is reduced by 74.1% when the initial tendon stress is increased from 0.45f_{pu} to 0.65f_{pu}. Eq. (27) implies the rigid rotaton θ_r, which represents the resilient rocking capacity of the wall, will decrease due to reduced ΔF_v. This can be seen in Fig. 11 that point LLP shfits to the left obviously with the increase of initial tendon stress.

5.2.2 Material types

High-strength steel strands cannot accommodate enough elongation in their elastic range due to its limited elongation capacity and therefore alternative tendons made of composite polymer materials are analyzed. Table 4 shows the material properties range of different tendons. Fig. 12 shows the skeleton curves of the VD-SCWs with four types of PT tendons (200Gpa for steel strands, 50Gpa for GFRP, 100Gpa for AFRP, 150Gpa for CFRP). The reduction in the elastic stiffness of tendons will not affect the global responses of VD-SCWs before point ELL but will cause a decrease in the stiffness of the system after this point. The wall stiffness after point ELL is reduced by 69.5% when the tendon stiffness is reduced by 75.0%. Moreover, the yielding and subsequent loss of pretension is avoided in the stage between point ELL and point CCC after the composite polymer materials are used, implying that the SC capacity of the wall is maintained when the wall is subjected to large drift loading.

6. Conclusion

The following conclusions can be drawn from the analyses:

- The total lateral displacement in different limit states of VD-SCWs is calculated as the summation of elastic portion, correction portion and rigid-body rotation portion. The proposed methods achieve an accurate prediction of the skeleton curves in the three test specimen. The equation for the point DEC of the wall is derived based on elastic theory and can predict the movement in the different position of the wall at this state. The calculation of point ELL considers the gap opening effects along the wall base and therefore have a better prediction compared to the Perez method. A simplified closed-form solution is proposed for the point LLP which avoids iterative process in the Perez method.

Both methods cannot capture the point CCC of TW2 and TW3 due to the cyclic deterioration in the test specimens.

- The effects of different damper parameters and tendon parameters on the lateral load responses are investigated using the proposed methods. To increase the energy dissipation of the wall, the activation force in the dampers should increase as much as possible when the SC capacity is ensured. The variation of damper stiffness has little effect on the lateral load response of the wall. The increasing initial stress in PT tendons leads to an increase in the SC ratio and the lateral resistance in the point ELL, but causing that the wall is vulnerable to the tendon yielding as the lateral loading increases. However, the high elastic elongation rate of composite polymer can delay the occurrence of the tendon yielding and therefore maintain the SC capacity of the wall subjected to large drift loading.

Acknowledgments

The research described in this paper was sponsored by \"National Key R&D Program of China" (2018YFC0705), \ "The Fundamental Research Funds for the Central Universities"(2242019K40083) and \"Postgraduate Research & Practice Innovation Program of Jiangsu Province"(KYCX17_0119). The supports are gratefully acknowledged.

References

Aaleti, S. and Sritharan, S. (2009), "A simplified analysis method for characterizing unbonded post-tensioned precast wall systems", *Eng. Struct.*, **31**(12), 2966-2975. https://doi.org/10.1016/j.engstruct.2009.07.024.

Abdalla, J. A., Saqan, E. I. and Hawileh, R. A. (2014), "Optimum seismic design of unbonded post-tensioned precast concrete walls using ANN", *Comput. Concrete*, **13**(4), 547-567. http://dx.doi.org/10.12989/cac.2014.13.4.547.

Armouti, N. S. (1993), "Seismic performance of precast concrete structural walls", Ph.D. Dissertation, Lehigh University, Bethlehem, PA.

Bai Y., Lin X. (2015), "Numerical simulation on seismic collapse of thin-walled steel moment frames considering post local buckling behavior", *Thin Wall. Struct.*, **94**, 424-434. https://doi.org/10.1016/j.tws.2015.04.033.

Bayat M., Abdollahzadeh G. (2011), "On the effect of the near field records on the steel braced frames equipped with energy dissipating devices", *Latin American J. Solids Struct.*, **8**(4), 429-443. http://dx.doi.org/10.1590/S1679-78252011000400004.

Bayat M., Abdollahzade G. (2011), "Analysis of the steel braced frames equipped with ADAS devices under the far field records", *Latin American J. Solids Struct.*, **8**(2), 163-181. http://dx.doi.org/10.1590/S1679-78252011000200004.

Bayat M., Bayat M. (2014), "Seismic behavior of special moment-resisting frames with energy dissipating devices under near source ground motions", *Steel Compos. Struct.*, **16**(5), 533-557. https://doi.org/10.12989/scs.2014.16.5.533.

Eatherton, M. R., Ma, X., Krawinkler, H., Mar, D., Billington, S., Hajjar, J. F. and Deierlein, G. G. (2014), "Design concepts for controlled rocking of self-centering steel-braced frames", *J. Struct. Eng.*, **140**(11), https://doi.org/10.1061/(ASCE)ST.1943-541X.0001047.

Erkmen, B. and Schultz, A. E. (2009), "Self-centering behavior of unbonded post-tensioned precast concrete shear walls", *J. Earthq. Eng.*, **13**(7), 1047-1064. https://doi.org/10.1080/13632460902859136.

Garlock, M. M., Ricles, J. M. and Sause, R. (2005), "Experimental studies of full-scale posttensioned steel connections", *J. Struct. Eng.*, **131**(3), 438-448. https://doi.org/10.1061/(ASCE)0733-9445(2005)131:3(438).

Guo, T., Xu, Z., Song, L., Wang, L. and Zhang, Z. (2017), "Seismic resilience upgrade of RC frame building using self-centering concrete walls with distributed friction devices", *J. Struct. Eng.*, **143**(12), https://doi.org/10.1061/(ASCE)ST.1943-541X.0001901

Guo, T., Zhang, G. and Chen, C. (2014), "Experimental study on self-centering concrete wall with distributed friction devices", *J. Earthq. Eng.*, **18**(2), 214-230. https://doi.org/10.1080/13632469.2013.844211.

Huang, X., Zhou, Z., Xie, Q., Xue, R. and Zhu, D. (2017), "Force distribution analysis of self-centering coupled-beams for moment-resisting-frames without floor elongation", *Eng. Struct.*, **147**, 328-344. https://doi.org/10.1016/j.engstruct.2017.05.055.

Hu, X., Zhang, Y. and Moghaddasi B, N. S. (2012), "Seismic performance of reinforced concrete frames retrofitted with self-centering hybrid wall", *Adv. Struct. Eng.*, **15**(12), 2131-2143.

Kim, H. J. and Christopoulos, C. (2008), "Friction damped posttensioned self-centering steel moment-resisting frames", *J. Struct. Eng.*, **134**(11), 1768-1779. https://doi.org/10.1061/(ASCE)0733-9445(2008)134:11(1768).

Kurama, Y.C. (2000) "Seismic design of unbonded post-tensioned precast concrete walls with supplemental viscous damping", *ACI Struct. J.*, **97**(4), 648-658.

Kurama, Y.C. (2001), "Simplified seismic design approach for friction-damped unbonded post-tensioned precast concrete walls", *ACI Struct. J.*, **98**(5), 705-716.

Kurama Y.C. (1997), "Seismic analysis, behavior and design of unbonded post-tensioned precast concrete walls", Ph.D. Dissertation, Lehigh University, Bethlehem, PA.

Kurama, Y., Sause, R., Pessiki, S. and Lu, L. W. (1999), "Lateral load behavior and seismic design of unbonded post-tensioned precast concrete walls", *ACI Struct. J.*, **96**(4), 622-632.

Kurama, Y.C., Sause, R., Pessiki, S. and Lu, L. W. (2002), "Seismic response evaluation of unbonded post-tensioned precast walls", *ACI Struct. J.*, **99**(5), 641-651.

Maurya A., Eatherton M.R. (2016), "Experimental study of the restoring force mechanism in the self-centering beam (SCB)", *Frontier. Struct. Civil Eng.*, **10**(3), 272-282. https://doi.org/10.1007/s11709-016-0346-x.

Priestley, M. N. and Tao, J. R. (1993), "Seismic response of precast prestressed concrete frames with partially debonded tendons", *PCI J.*, **38**(1), 58-69.

Perez FJ, Pessiki S, Sause R. (2004a) "Experimental and analytical lateral load response of unbonded post-tensioned precast concrete walls", ATLSS Report No. 04-11; Department of Civil Engineering, Lehigh University.

Perez, F. J., Pessiki, S. and Sause, R. (2004b), "Seismic design of unbonded post-tensioned precast concrete walls with vertical joint connectors", *PCI J.*, **49**(1), 58-79.

Perez, F. J., Pessiki, S. and Sause, R. (2004c), "Lateral load behavior of unbonded post-tensioned precast concrete walls with vertical joints", *PCI J.*, **49**(2), 48-64.

Perez, F. J., Pessiki, S. and Sause, R. (2013), "Experimental lateral load response of unbonded post-tensioned precast concrete walls", *ACI Struct. J.*, **110**(6), 1045-1055.

Perez, F. J., Sause, R. and Pessiki, S. (2007), "Analytical and experimental lateral load behavior of unbonded posttensioned precast concrete walls", *J. Struct. Eng.*, **133**(11), 1531-1540. https://doi.org/10.1061/(ASCE)0733-9445(2007)133:11(1531).

Qiu, C. and Zhu, S. (2017), "Shake table test and numerical study of self-centering steel frame with SMA braces", *Earthq*. *Eng*. *Struct*. *Dynam*., **46**(1), 117-137. https://doi.org/10.1002/eqe.2777.

Restrepo, J. I. and Rahman, A. (2007), "Seismic performance of self-centering structural walls incorporating energy dissipators", *J*. *Struct*. *Eng*., **133**(11), 1560-1570. https://doi.org/10.1061/(ASCE)0733-9445(2007)133:11(1560).

Sritharan S, Aaleti S, Thomas D (2007) "Seismic analysis and design of precast concrete jointed wall systems", *ISU-ERI-Ames report*, Ames (Iowa), Department of Civil, Construction and Environmental Engineering, Iowa State University.

Thomas DJ, Sritharan S. (2004), "An evaluation of seismic design guidelines proposed precast jointed wall systems", *ISU-ERI-Ames report ERI-04643*, Ames (Iowa), Department of Civil and Construction and Environmental Engineering, Iowa State University.

Xue, J., Qi, L., Yang, K. and Wu, Z. (2017), "Dynamic experimental study on single and double beam-column joints in steel traditional-style buildings", *Struct*. *Eng*. *Mech*., **63**(5), 617-628. https://doi.org/10.12989/sem.2017.63.5.617.

Xue, J., Bai, F., Qi, L., Sui, Y. and Zhou, C. (2018), "Research on damage and identification of mortise-tenon joints stiffness in ancient wooden buildings based on shaking table test", *Struct*. *Eng*. *Mech*., **65**(5), 547-556. https://doi.org/10.12989/sem.2018.65.5.547

Zhou, Z., Xie, Q., Lei, X.C., He, X.T. and Meng, S.P. (2015), "Experimental investigation of the hysteretic performance of dual-tube self-centering buckling-restrained braces with composite tendons", *J*. *Compos*. *Construct*., **19**(6), https://doi.org/10.1061/(ASCE)CC.1943-5614.0000565.

PL